Numerical study of magnetization plateaus in the spin-$\frac{1}{2}$ kagome Heisenberg antiferromagnet

Sylvain Capponi,[1] Oleg Derzhko,[2,3,4] Andreas Honecker,[5,6] Andreas M. Läuchli,[7] and Johannes Richter[8]

[1]*Laboratoire de Physique Théorique, Université de Toulouse and CNRS, UPS (IRSAMC), F-31062 Toulouse, France*

[2]*Institute for Condensed Matter Physics, National Academy of Sciences of Ukraine, 1 Svientsitskii Street, L'viv-11 79011, Ukraine*

[3]*Department for Theoretical Physics, Ivan Franko National University of L'viv, 12 Drahomanov Street, L'viv-5 79005, Ukraine*

[4]*Abdus Salam International Centre for Theoretical Physics, Strada Costiera 11, I-34151 Trieste, Italy*

[5]*Institut für Theoretische Physik, Georg-August-Universität Göttingen, D-37077 Göttingen, Germany*

[6]*Fakultät für Mathematik und Informatik, Georg-August-Universität Göttingen, D-37073 Göttingen, Germany*

[7]*Institut für Theoretische Physik, Universität Innsbruck, A-6020 Innsbruck, Austria*

[8]*Institut für Theoretische Physik, Otto-von-Guericke-Universität Magdeburg, P. O. Box 4120, D-39016 Magdeburg, Germany*

(Received 8 July 2013; revised manuscript received 16 September 2013; published 18 October 2013)

We clarify the existence of several magnetization plateaus for the kagome $S = \frac{1}{2}$ antiferromagnetic Heisenberg model in a magnetic field. Using approximate or exact localized magnon eigenstates, we are able to describe in a similar manner the plateau states that occur for magnetization per site $m = \frac{1}{3}$, $\frac{5}{9}$, and $\frac{7}{9}$ of the saturation value. These results are confirmed using large-scale exact diagonalization on lattices up to 63 sites.

DOI: 10.1103/PhysRevB.88.144416 PACS number(s): 75.10.Jm, 75.40.Mg

I. INTRODUCTION

When the kagome lattice was introduced, it was shown that the antiferromagnetic Ising model on this lattice does not order.[1] Until today, the kagome lattice remains a classic problem in highly frustrated magnetism.[2] One of the open problems concerns the physics of the spin-$\frac{1}{2}$ Heisenberg model on the kagome lattice in zero field, where despite several numerical[3–7] and variational studies,[8] the situation is still not fully understood. The most recent density matrix renormalization group (DMRG) studies point towards a translationally invariant spin-liquid state[9,10] with no apparent broken symmetries, a gap to triplet excitations of order $\Delta_{S=1} = 0.13\,J$ and short-range spin correlations. This state is consistent with a resonating valence bond (RVB) state[11] with $\mathbb{Z}_2$ topological order.[10,12]

Returning to the Ising model on the kagome lattice, the zero-field ground state is known to be highly degenerate.[13] Application of a small longitudinal magnetic field polarizes one third of the spins, but remarkably a macroscopic ground-state degeneracy survives. Only further inclusion of quantum fluctuations lifts this degeneracy and gives rise to a state with quantum order of valence bond crystal (VBC) type.[14,15] This VBC state is accompanied by a pronounced plateau in the magnetization curve at $\frac{1}{3}$ of the saturation magnetization. A similar $\frac{1}{3}$ plateau was also observed in the spin-$\frac{1}{2}$ Heisenberg antiferromagnet on the kagome lattice.[16–19] It was further argued that the states of the $\frac{1}{3}$ plateau at the Heisenberg point and close to the Ising limit belong to the same phase.[15,20] Exchange anisotropy has also been shown to stabilize a $\frac{1}{3}$ plateau in the classical limit $S = \infty$.[21] More recently, however, the very existence of this $\frac{1}{3}$ plateau in the spin-$\frac{1}{2}$ Heisenberg model was challenged.[22–25] In this context, it is noteworthy that a plateau close but not exactly equal to magnetization $m = \frac{1}{3}$ has been observed experimentally in two kagome compounds.[26]

At very high magnetic fields, one can rigorously construct a macroscopic number of quantum ground states for a class of highly frustrated lattices including the kagome lattice.[17,18,27–30] These exact ground states arise just below the saturation field and are accompanied by a jump in the magnetization curve of height $\Delta m = 1/(9\,S)$ and a plateau just below this jump. For $S = \frac{1}{2}$, the magnetization value on this plateau is $m = \frac{7}{9}$. Since the ground states are known exactly, one can rigorously show that this high-field plateau exhibits the order sketched in Fig. 1: in a background of polarized ("up") spins, one flipped ("down") spin is localized in a quantum superposition on each hexagon marked by a dashed circle in Fig. 1. Note that the same global structure has been argued to hold at $m = \frac{1}{3}$,[15,20] just the resonances in the hexagons are between three up and three down spins for $m = \frac{1}{3}$. The states on both plateaus are indeed consistent with a two-dimensional generalization[31] of a commensurability criterion.[32] This criterion would allow further for an $m = \frac{5}{9}$ plateau and, indeed, the same structure as is sketched in Fig. 1 suggests itself at $m = \frac{5}{9}$ if one now considers two down and four up spins on each hexagon. The possibility of an $m = \frac{5}{9}$ plateau was mentioned previously,[19] but has not been investigated systematically yet.

The aim of this paper is to provide a further analysis of the $m = \frac{1}{3}$, $\frac{5}{9}$, and $\frac{7}{9}$ plateaus. To be concrete, we focus on the antiferromagnetic spin-$\frac{1}{2}$ Heisenberg model on the kagome lattice

$$\mathcal{H} = J \sum_{\langle ij \rangle} \boldsymbol{S}_i \cdot \boldsymbol{S}_j - h \sum_i S_i^z \,. \tag{1}$$

$J > 0$ is taken as the unit of energy and h is the magnetic field along the z direction. We will denote the magnetization per site by $m = 2\,S^z/N$, where S^z is the z component of the total spin and N the number of sites. This normalization ensures a saturation value $m = 1$.

Before we proceed, we mention that similar physics arises in bosonic models on the kagome lattice,[33,34] opening a further route for experimental realizations via ultracold atoms in optical lattices.[35,36]

The remainder of the paper is organized as follows: in Sec. II, we generalize the exact wave function of the $m = \frac{7}{9}$ plateau to variational VBC wave functions for the candidate plateaus at $m = \frac{1}{3}$ and $\frac{5}{9}$. In Sec. III, we perform extensive

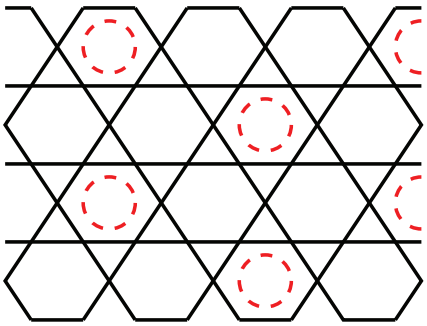

FIG. 1. (Color online) Visualization of the valence bond crystal type states for the $m = \frac{3}{9}, \frac{5}{9}$, and $\frac{7}{9}$ plateaus in the $S = \frac{1}{2}$ Heisenberg antiferromagnet on the kagome lattice.

exact diagonalization (ED) on various lattices to confirm (i) the existence of these three plateaus and (ii) their VBC nature.

II. VARIATIONAL MODEL WAVE FUNCTIONS

In this section, we will write variational wave functions for the spin-$\frac{1}{2}$ model (1) on the kagome lattice at $m = \frac{1}{3}$ and $\frac{5}{9}$, following the example of the exactly known eigenstates with $S^z \geqslant N/2 - N/9$.[17,27–30,37] The crucial ingredients of the exact construction are "independent" localized-magnon states where the magnons are strictly localized on the hexagons.

The independent localized-magnon state for $S^z = 7N/18$, i.e., $m = \frac{7}{9}$, is the so-called magnon-crystal state

$$\left|\Psi_{\mathrm{VBC}}^{7/9}\right\rangle = \prod_j |L,\downarrow\rangle_j \prod_l |\uparrow\rangle_l \tag{2}$$

(see Fig. 1). Here, the first product runs over an ordered pattern of all nonoverlapping hexagons denoted by the dashed circles in Fig. 1 and the second product runs over the remaining sites. The localized-magnon state on a hexagon (which is the lowest-energy state of a hexagon with one spin flipped) is

$$|L,\downarrow\rangle = \|\downarrow\uparrow\uparrow\uparrow\uparrow\uparrow\rangle\!\rangle_\pi \,. \tag{3}$$

For convenience, we have introduced here the momentum eigenstate for a hexagon

$$\|\sigma_0 \ldots \sigma_5\rangle\!\rangle_k := \frac{1}{\sqrt{\mathcal{N}}} \sum_{r=0}^{5} \exp(i\,k\,r)\,|\sigma_r \ldots \sigma_{5+r}\rangle \,, \tag{4}$$

where $\sigma_n = \downarrow, \uparrow$, $n + r$ has to be read modulo 6, and $\mathcal{N}$ is a normalization factor ensuring ${}_k\langle\!\langle\sigma_0 \ldots \sigma_5\|\sigma_0 \ldots \sigma_5\rangle\!\rangle_k = 1$ ($\mathcal{N} = 6$ unless the state repeats under less than 6 translations).

One can show that the state (2), (3) is not only an exact threefold-degenerate eigenstate of the Hamiltonian $\mathcal{H}$ (1), but also a ground state in the subspace with $S^z = 7N/18$.[37] Its energy per site at $h = 0$ is $e_{\mathrm{VBC}}^{7/9}/J = \frac{1}{6}$. From general arguments,[38] the magnon-crystal state (2), (3) should have gapped excitations that lead to a plateau at $m = \frac{7}{9}$.

On the other hand, it has been argued[15] that the $\frac{1}{3}$ plateau is described by a similar wave function. The global pattern of resonances is again as sketched in Fig. 1, but now the dashed circles represent a combination of the two Néel states on a hexagon. This provides a quantitative description for the $m = \frac{1}{3}$ state of the $S = \frac{1}{2}$ XXZ Heisenberg model in the limit of large values of the Ising anisotropy Δ.[15] Although overlaps of the wave functions indicate that this remains qualitatively correct for the isotropic case $\Delta = 1$,[15] it may still be better to consider the lowest-energy singlet state of the Heisenberg model on the hexagon $|L,\downarrow\downarrow\downarrow\rangle$. Hence, the corresponding threefold-degenerate valence bond crystal model state in the subspace with $S^z = 3N/18$ reads as

$$\left|\Psi_{\mathrm{VBC}}^{3/9}\right\rangle = \prod_j |L,\downarrow\downarrow\downarrow\rangle_j \prod_l |\uparrow\rangle_l \,. \tag{5}$$

The six-spin Heisenberg ring is easily diagonalized and one finds

$$\begin{aligned} |L,\downarrow\downarrow\downarrow\rangle = \frac{1}{\sqrt{195 + 51\sqrt{13}}}\Big[& 3\,\|\downarrow\downarrow\downarrow\uparrow\uparrow\uparrow\rangle\!\rangle_\pi \\ & + \frac{3\,(3+\sqrt{13})}{2}\,(\|\downarrow\downarrow\uparrow\uparrow\downarrow\uparrow\rangle\!\rangle_\pi - \|\downarrow\downarrow\uparrow\downarrow\uparrow\uparrow\rangle\!\rangle_\pi) \\ & + \sqrt{3}(4+\sqrt{13})\,\|\uparrow\downarrow\uparrow\downarrow\uparrow\downarrow\rangle\!\rangle_\pi \Big]. \end{aligned} \tag{6}$$

Although the state (5), (6) is not an exact eigenstate of the Hamiltonian $\mathcal{H}$ (1), it is a good model for the true ground state in the subspace with $S^z = 3N/18$ (see following). The variational energy of this state at $h = 0$ is $e_{\mathrm{VBC}}^{1/3}/J = -1/9 - \sqrt{13}/18 = -0.311\,419\,515\,3$ per site. This is considerably lower than the *variational* estimate $e_{\mathrm{Ising}}^{1/3} = 0$ derived from the superposition of the two Néel states.[15] Consequently, the state (5), (6) is closer to the true ground state for $\Delta = 1$.

Inspired by the valence bond crystal states (2), (3) and (5), (6) for the plateaus at $m = \frac{7}{9}$ and $\frac{3}{9}$, respectively, it is natural to propose a new variational wave function at $m = \frac{5}{9}$:

$$\left|\Psi_{\mathrm{VBC}}^{5/9}\right\rangle = \prod_j |L,\downarrow\downarrow\rangle_j \prod_l |\uparrow\rangle_l \tag{7}$$

with

$$\begin{aligned} |L,\downarrow\downarrow\rangle = \frac{1}{2\sqrt{5}}[& (\sqrt{5}-1)\|\uparrow\uparrow\uparrow\uparrow\downarrow\downarrow\rangle\!\rangle_0 \\ & - (\sqrt{5}+1)\,\|\uparrow\uparrow\uparrow\downarrow\uparrow\downarrow\rangle\!\rangle_0 \\ & + 2\sqrt{2}\,\|\uparrow\uparrow\downarrow\uparrow\uparrow\downarrow\rangle\!\rangle_0]. \end{aligned} \tag{8}$$

The variational energy of this state at $h = 0$ is $e_{\mathrm{VBC}}^{5/9}/J = -\sqrt{5}/18 = -0.124\,225\,998\,7$ per site. Again, this is not an exact eigenstate of the Hamiltonian $\mathcal{H}$ (1), however, it is not far from the true ground state as extensive numerics show (see following).

It should be noted that in all three cases, the wave functions are threefold degenerate. They can provide a number of consequences for correlations which in turn can be checked by exact diagonalization (ED). In particular, in view of their crystalline nature, we expect a finite gap and thus a plateau in the magnetization curve not only for $m = \frac{7}{9}$, but also for $m = \frac{1}{3}$ and $\frac{5}{9}$.

In the following, we present ED for finite systems and by comparison with theoretical predictions based on the variational wave functions (5), (6) and (7), (8) demonstrate that these model states provide a good description of the physics within the plateau regimes.

III. NUMERICAL RESULTS

We have performed extensive exact diagonalization using the Lanczos algorithm in order to compute the magnetization curve for various lattices. Following Ref. 6, we consider a large variety of finite lattices using periodic boundary conditions (PBC), including also less symmetric ones that can not accommodate the expected VBC, in order to analyze finite-size effects. Also, since the existence of short loops going around the lattices are the major finite-size effects, we perform the finite-size scaling using the geometric length, i.e., the smallest distance around the torus. Definitions of lattices and geometric distance are given in the Appendix.

A. Magnetization curves

Since we are considering states with a large magnetization, we have to deal with smaller Hilbert spaces than in $S^z = 0$, which means that we can access larger lattices. In this study, we have considered lattices up to $N = 63$ for which we can compute some part of the magnetization curve. Given the number of data, we do not plot all system sizes, but Fig. 2 shows part of the magnetization curves for lattices that accommodate the VBC discussed in Sec. II. We recover some known features, such as the exact saturation field $h = 3J$ that can be understood in terms of the localized magnon eigenstates and a jump to $m = \frac{7}{9}$. For this plateau, we have considered more lattices than previously in the literature, and we already see on the plot that its width seems to saturate as system size increases. A detailed analysis will be performed in the following. Similarly, looking at the $m = \frac{1}{3}$ and $\frac{5}{9}$ finite-size plateaus it seems that finite-size effects are rather weak both for the width and the location of these plateaus.

Focusing on the expected plateaus at $m = \frac{1}{3}$, $\frac{5}{9}$, and $\frac{7}{9}$, we plot their widths in Fig. 3 as a function of the inverse diameter which we believe is the relevant parameter. First of all, we do observe some variations of the data and peculiar results for the smallest lattices, but if we rely on the largest lattices (in the sense of their diameter, see Appendix), then we do observe a tendency to saturation to finite values for all three plateaus. Moreover, since our scenario relies on the existence of VBC states that *do not fit* on all lattices (for instance, the unit cell has 9 sites so clusters need to have $9p$ sites), it is not expected *a priori* to have similar widths on different lattices, which could explain some scattering in the data. Therefore, we consider only lattices having the K point in the Brillouin zone (see inset of Fig. 4 for a plot of the Brillouin zone).

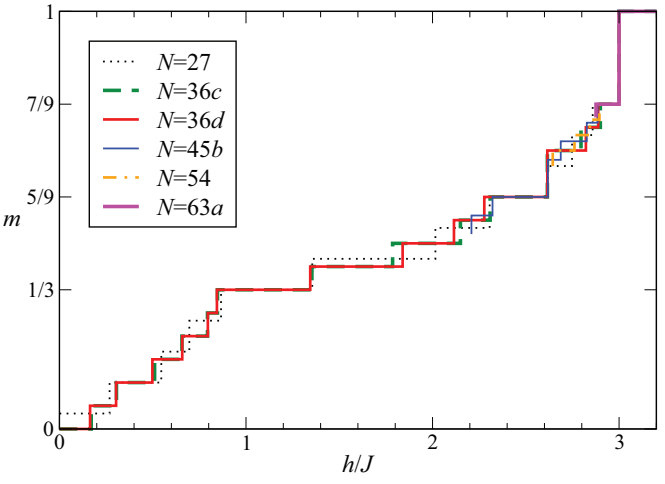

FIG. 2. (Color online) Magnetization curve of the $S = \frac{1}{2}$ kagome Heisenberg model on various lattices that can accommodate the VBC shown in Fig. 1 (see Appendix for details).

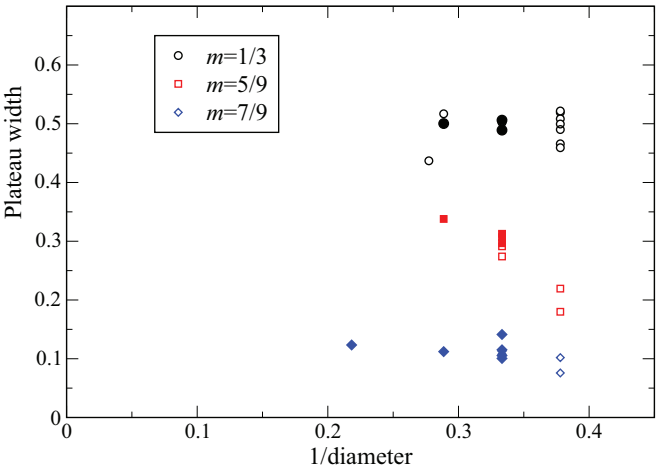

FIG. 3. (Color online) Widths of the $m = \frac{1}{3}$, $\frac{5}{9}$, and $\frac{7}{9}$ plateaus obtained from exact diagonalization on various lattices (see Appendix for a list), plotted as a function of the inverse diameter. Filled symbols correspond to lattices that can accommodate the VBC states, i.e., possess the K point in their Brillouin zone: 27, 36c, 36d, 45b, 54, and 63a. Open symbols are for the others. Data are consistent with finite values for all three plateaus in the thermodynamic limit.

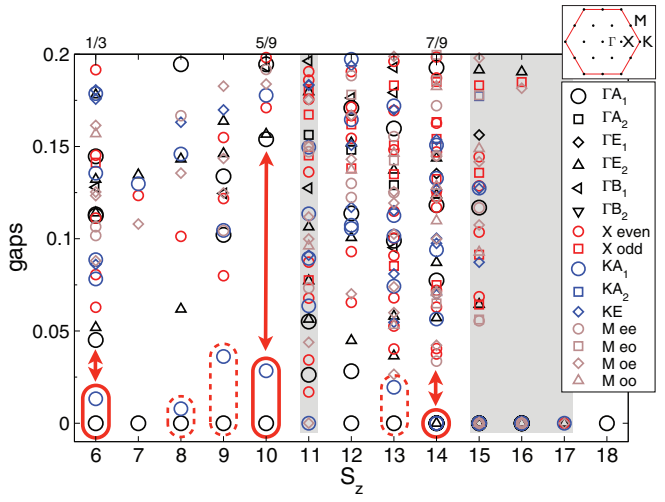

FIG. 4. (Color online) Energy gaps vs S^z for $N = 36d$ lattice labeled with their quantum numbers. For $S^z = 6$, 10, and 14 corresponding, respectively, to $m = \frac{1}{3}$, $\frac{5}{9}$, and $\frac{7}{9}$, the lowest excitation corresponds to a twofold-degenerate state at the K point in the Brillouin zone, and then a sizable gap above it (indicated by the encircled symbols and the arrows). These spectra are compatible with the VBC states for such magnetizations. The dashed encircled symbols denote levels which might indicate persistence of symmetry breaking also away from the nominal plateaus. The magnetization sectors with a gray background are not visited in the magnetization curve, i.e., they are obscured by a magnetization jump.

In order to perform finite-size scaling, it does not seem appropriate to us to use a simple linear fit extrapolation as done in Ref. 23. Indeed, for a finite plateau, one expects an exponential saturation when the system size (or diameter) increases. Hence, by performing such extrapolation of our data, we obtain *finite* plateaus for $m = \frac{1}{3}$, $\frac{5}{9}$, and $\frac{7}{9}$, with decreasing widths of the order of $0.5\,J$, $0.3\,J$, and $0.1\,J$, respectively. For $m = \frac{7}{9}$, this new estimate for the plateau width is actually slightly larger than a previous estimate[39] $0.07\,J$.

B. Energetics

In order to characterize possible symmetry breaking, it is useful to investigate the low-energy levels quantum numbers on a finite lattice. For instance, according to Sec. II, we expect to have VBC states on these plateaus with threefold degeneracy. In the thermodynamic limit, this implies that we have degeneracy between states at the Γ point (ΓA_1) and the twofold-degenerate K point (KA_1). In Fig. 4, we plot the energy gaps obtained by computing the 10 lowest eigenstates in each symmetry sector using a Davidson algorithm. We have subtracted the ground-state energy for each S^z, but for comparison with the variational VBC states, let us mention that on $N = 36d$ lattice, the ground-state energy per site for $m = \frac{1}{3}$ is $e_0 = -0.347\,711\,J$, for $m = \frac{5}{9}$: $e_0 = -0.137\,251\,J$, and for $m = \frac{7}{9}$ we get the exact VBC state with $e_0 = J/6$. Therefore, our simple VBC wave functions (without any adjustable parameter) already give a reasonable estimate of these ground-state energies.

About the excited states shown in Fig. 4, exact degenerate magnon eigenstates are found for $m \geqslant \frac{7}{9}$ as expected. For $m = \frac{7}{9}$ (i.e., $S^z = 14$), the ground state is more than threefold degenerate due to small loops going around the lattice (on $N = 63a$, degeneracy is exactly three, see below), but there is evidence of a small gap above them. At $m = \frac{5}{9}$ ($S^z = 10$), we do observe twofold-degenerate states with momentum K close to the Γ ground state, and a sizable gap above them.

Let us also mention a possible feature below the $m = \frac{5}{9}$ plateau: on the low-energy spectrum, we observe the same feature as on the plateau, which could signal the persistence of VBC order *away* from this magnetization. However, since we expect that the magnetization decreases smoothly from the plateau, such a state could possibly exhibit both off-diagonal and diagonal long-range order, i.e., a supersolid state.[40] One has to be cautious about this scenario since other possibilities exist such as the absence of superfluid signal, or magnetization jump. Nevertheless, we believe that this would be an interesting topic to investigate further. For instance, simple bosonic models on the same lattice only exhibit plateaus at $\frac{1}{3}$, and there is no supersolid phase.[41]

As a conclusion on this part, we have shown that the low-energy spectrum points towards a VBC scenario, which we will now confirm by directly computing relevant correlations.

C. Correlations

Having established the existence of these three plateaus, we now turn to their characterization. Let us remind that according to Hastings' theorem,[31] $m = \frac{5}{9}$ and $\frac{7}{9}$ plateaus necessarily correspond to a (at least threefold-) degenerate ground state. While exotic scenarios with topological degeneracy are possible, the more usual case is to have a system that breaks lattice symmetries. This is not necessarily the case for $m = \frac{1}{3}$, but our arguments (see Sec. II) indicate that all three plateaus correspond to similar threefold-degenerate VBC states.

For each magnetization m, we have computed connected spin correlation functions

$$\left\langle S_i^z S_j^z \right\rangle_c = \left\langle S_i^z S_j^z \right\rangle - \left\langle S_i^z \right\rangle \left\langle S_j^z \right\rangle \tag{9}$$

as well as connected dimer-dimer correlations

$$\begin{aligned} &\langle (\boldsymbol{S}_i \cdot \boldsymbol{S}_j)(\boldsymbol{S}_k \cdot \boldsymbol{S}_\ell) \rangle_c \\ &\quad = \langle (\boldsymbol{S}_i \cdot \boldsymbol{S}_j)(\boldsymbol{S}_k \cdot \boldsymbol{S}_\ell) \rangle - \langle (\boldsymbol{S}_i \cdot \boldsymbol{S}_j) \rangle \langle (\boldsymbol{S}_k \cdot \boldsymbol{S}_\ell) \rangle \end{aligned} \tag{10}$$

using ED on the $N = 36d$ lattice for $m = \frac{1}{3}$ and $\frac{5}{9}$, and the $N = 63a$ lattice for $m = \frac{7}{9}$. These are the largest lattices (in the sense of their diameter, see Appendix) available for each m value. Data are presented in Fig. 5.

In order to make a more precise connection with our VBC picture, we have also computed the same quantities on the pure states as shown in Fig. 1. For each m, we have three degenerate states that are orthogonal in the thermodynamic limit, so that we can choose to symmetrize them (for instance, in the fully symmetric irreducible representation) in order to construct a uniform state. Equivalently, one can choose one VBC state and then average over distances. To perform these computations is a bit tedious but straightforward. We give here some details on the calculation, and relevant results are shown in Tables I and II.

For spin correlations, if sites i and j belong to the same hexagon, then correlations can be obtained from the hexagon wave functions given in Eqs. (3), (6), and (8); if site i corresponds to a polarized site (resp. resonating hexagon), then $\langle S_i^z \rangle = \frac{1}{2}$ [resp. $(9m-3)/12$]. If sites i and j are sufficiently distant, then correlation simply factorizes since we have a product state. As an example for $m = \frac{7}{9}$, the nearest-neighbor spin correlations are given by

$$\left(\frac{1}{12} + 2 \times \frac{1}{3} \times \frac{1}{2}\right) \Big/ 3 - \left(\frac{m}{2}\right)^2 = -\frac{1}{81},$$

while at large distance we find only two different values

$$\left(\frac{1}{3} \times \frac{1}{2} + \frac{1}{3} \times \frac{1}{2} + \frac{1}{3} \times \frac{1}{3}\right) - \left(\frac{m}{2}\right)^2 = -\frac{1}{324}$$

and

$$\left(\frac{1}{3} \times \frac{1}{3} + \frac{1}{3} \times \frac{1}{3} + \frac{1}{2} \times \frac{1}{2}\right) - \left(\frac{m}{2}\right)^2 = \frac{1}{162},$$

and similar computations can be performed for other m and distances.

Dimer correlation can be computed in a similar way, but since we have many possibilities for (ij) and $(k\ell)$ bonds, we will not give all numbers. We need to compute $\langle (\boldsymbol{S}_i \cdot \boldsymbol{S}_j) \rangle$: when i and j are nearest neighbors inside one resonating hexagon, then this is simply the energy per bond for the wave functions (3), (6), and (8); in the other case, one site is necessarily a polarized one so that correlations reduce to $\langle S_i^z S_j^z \rangle = \langle S_i^z \rangle \langle S_j^z \rangle = (9m-3)/24$. Let us denote these two values as d_1 and d_2. If we neglect short-distance effects that require detailed computation (10 different relative bond

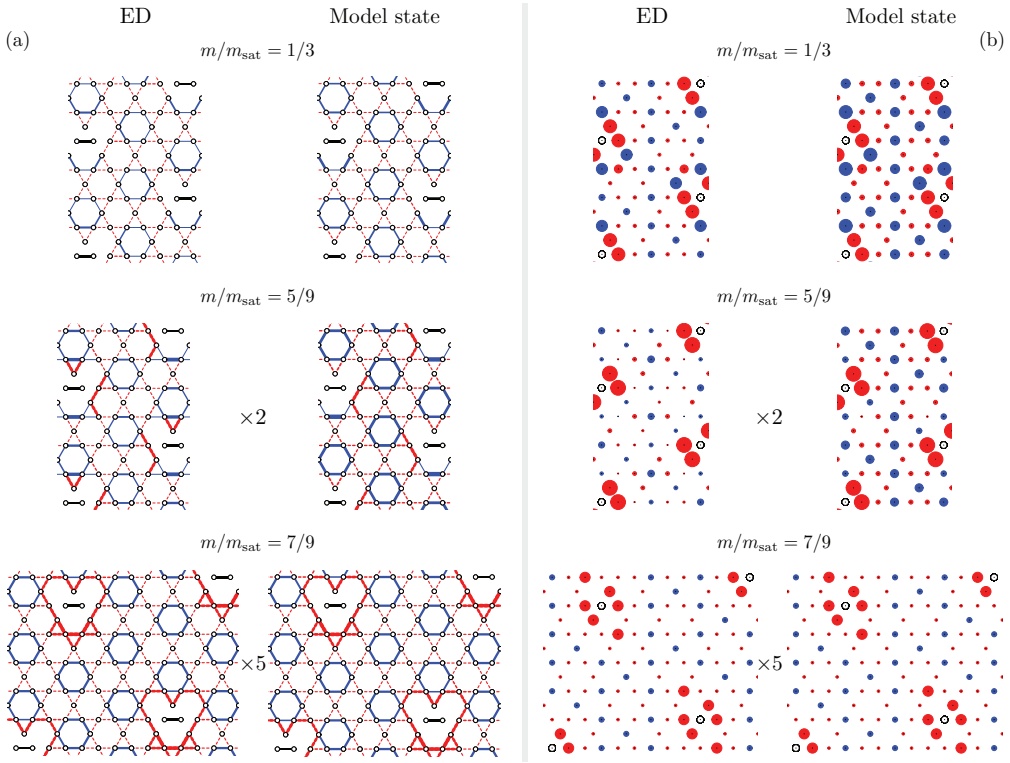

FIG. 5. (Color online) Dimer and spin correlations (see text for definitions) computed either by ED or on the magnon VBC state for various magnetizations: on $N = 36d$ for $m = \frac{1}{3}$ and $\frac{5}{9}$, on $N = 63a$ for $m = \frac{7}{9}$. (a) Dimer-dimer correlations [cf. Eq. (10)]: positive and negative values are shown, respectively, with filled blue lines (respectively dashed red lines) and width is proportional to the data (see Table II); reference bond is shown in black. (b) Spin correlations [cf. Eq. (9)]: positive and negative values are shown, respectively, with filled blue (resp. red) disks and diameter is proportional to the data (see Table I); the reference site is shown as an empty black circle. In order to have similar amplitudes, scale is multiplied by 2 and 5 for $m = \frac{5}{9}$ and $\frac{7}{9}$ with respect to $m = \frac{1}{3}$ data.

positions), then computations are much simpler and we have found only two cases:

$$\left(d_1 d_2 + 2d_2^2\right)/3 - \left(\frac{d_1 + 2d_2}{3}\right)^2$$

and

$$\left(d_1^2 + 2d_2^2\right)/3 - \left(\frac{d_1 + 2d_2}{3}\right)^2.$$

As an example for $m = \frac{7}{9}$, we obtain respectively $-\frac{1}{144}$ and $\frac{1}{72}$. Some of these numbers are reported in Table II.

$m = \frac{7}{9}$ plateau. We observe degeneracies larger than three on small lattices presumably due to the existence of short loops around them (compare also Ref. 30). However, using our largest $N = 63a$ lattice of which the diameter is $d = \sqrt{21}$, we do confirm that the ground state at $m = \frac{7}{9}$ is exactly threefold degenerate (corresponding to the three possible VBC), so that one can form eigenstates with momentum Γ and twofold states with K. Our numerical correlations perfectly agree with our analytical results performed on the VBC states, and tiny differences can be attributed to the small overlap between the three magnon states on a finite lattice. Data are plotted in Fig. 5, which is a perfect signature of the existence of a VBC state.

$m = \frac{5}{9}$ plateau. In this case, we consider lattice $N = 36d$. Although spin and dimer correlations are a bit less intense than

TABLE I. Connected $\langle S_i^z S_j^z \rangle_c$ for i, j inside one hexagon at Manhattan distance d or along one direction for various VBC states corresponding to different m.

	Same hexagon			Along one direction	
$\langle S_i^z S_j^z \rangle_c$	$d = 1$	$d = 2$	$d = 3$	$d = 2$	$d = 3$
$m = 7/9$	$-1/81$	$-1/324$	$-1/81$	$-1/324$	$1/162$
$m = 5/9$	-0.045	0.0167	-0.005	$-1/81$	$2/81$
$m = 1/3$	-0.0797	0.0787	-0.053	$-1/36$	$1/18$

TABLE II. Connected $\langle (\boldsymbol{S}_i \cdot \boldsymbol{S}_j)(\boldsymbol{S}_k \cdot \boldsymbol{S}_\ell) \rangle_c$ for a fixed reference bond (i, j) and various bonds (k, ℓ) either belonging to the same hexagon at Manhattan distance d or not. Other relative bond positions are possible so that 12 different values can be found. Here, we show only four different values for each VBC corresponding to different m.

	Same hexagon		Different hexagon	
$\langle (\boldsymbol{S}_i \cdot \boldsymbol{S}_j)(\boldsymbol{S}_k \cdot \boldsymbol{S}_\ell) \rangle_c$	$d = 1$	$d = 2$	Positive	Negative
$m = 7/9$	$-5/216$	$-5/216$	$-1/144$	$1/72$
$m = 5/9$	$0.066\,55$	$0.016\,30$	$-0.041\,54$	$0.021\,92$
$m = 1/3$	$0.029\,74$	$0.079\,46$	$-0.024\,24$	$0.048\,49$

in the pure VBC state (we know that this is not an eigenstate anymore), both the sign patterns and the long-range order are in very good agreement. This leads us to the conclusion that for $m = \frac{5}{9}$ a VBC state emerges, and since this is a gapped state, we expect a finite plateau at this magnetization.

$m = \frac{1}{3}$ plateau. The same conclusion seems to be valid for $m = \frac{1}{3}$ where correlations have a similar pattern to those found in the pure VBC state. Both short-distance properties of the VBC wave function are recovered in ED data, but also the fact that correlations do not depend much on distance and seem to remain finite.

IV. CONCLUSION

We have shown that the kagome antiferromagnet in strong magnetic field exhibits a nontrivial magnetization curve. Previous studies had indicated that plateaus should exist for $m = \frac{1}{3}$ and $\frac{7}{9}$ of its saturation value, but recently the existence of the $\frac{1}{3}$ plateau has been challenged.[22–25] Here, we have not only presented further support for the existence of the $\frac{1}{3}$ plateau, but also evidence in favor of an $m = \frac{5}{9}$ plateau, in addition to the exactly known $\frac{7}{9}$ plateau. We have presented a unified view of these plateau states, which are valence bond crystals that break lattice symmetries.

Our approach is based on a generalization of the exact magnon-crystal state which exists at $m = \frac{7}{9}$, which we believe captures as well the physics for the other plateaus. These wave functions correspond to simple VBC states such as depicted in Fig. 1 where resonating hexagons have a fixed magnetization equal to 0, 1, and 2, respectively, and they share similar properties.

Our exact diagonalizations on large lattices have confirmed (i) that these three plateaus have a finite extent in the thermodynamic limit, of widths roughly equal to $0.5\,J$, $0.3\,J$, and $0.1\,J$, respectively; (ii) for these magnetizations, the ground state is threefold degenerate and corresponds to the expected VBC state. Last but not least, both spin and dimer correlations are in very good agreement with the magnon VBC state, which allows us to present a simple physical picture of these three gapped phases.

Since for $m = \frac{1}{3}$ it is possible to construct a featureless bosonic state on this lattice[36] (i.e., a unique quantum Mott insulator of bosons that has no broken symmetry or topological order), it would be interesting to look for models that can interpolate between having a VBC ground state or a featureless one. In this context, more work should be devoted to understand the difference between Heisenberg and bosonic models, and also to investigate whether supersolid phases are stable or not.

Let us finally mention that the localized-magnon scenario holds for a quite large variety of one-, two-, and three-dimensional frustrated lattices.[29,30] Hence, we may argue that our VBC approach based on a generalization of the exact magnon-crystal state might be applicable to other lattices, such as the star lattice,[18,42–44] the sorrel net,[45,46] or the square-kagome lattice.[46–48] Moreover, it is known that also for spin quantum numbers $S > \frac{1}{2}$ and for anisotropic XXZ antiferromagnets the magnon-crystal state exists.[17,29,30] Therefore, the investigation of plateau states for other lattices and/or spin-S XXZ models is a fruitful field for further studies.

Note added in proof. Recently, we learned about Ref. 49 where magnetization plateaus are investigated with the density matrix renormalization group algorithm. These results agree with ours for the three plateaus that we have investigated, namely, that they correspond to valence bond crystals. Moreover, Ref. 49 predicts an exotic quantum plateau at $m = \frac{1}{9}$.

ACKNOWLEDGMENTS

Numerical simulations were performed at CALMIP and GENCI. O.D. would like to thank the Abdus Salam International Centre for Theoretical Physics (Trieste, Italy) for partial support of these studies through the Senior Associate award. A.H. and A.M.L. acknowledge support through DFG Grant No. HO 2325/9-1 and FWF Grant No. I1310-N27 (Forschergruppe FOR1807) and J.R. and O.D. through Grant No. RI 615/21-1 (DFG).

APPENDIX: LATTICE GEOMETRIES

Since we are using several kinds of lattices, we give their definitions using **a** and **b** translations to define the torus with periodic boundary conditions. Unit length corresponds to the Bravais lattice unit, i.e., two lattice spacings. We define the diameter of each lattice as $d = \min(|\mathbf{a}|, |\mathbf{b}|, |\mathbf{a} - \mathbf{b}|)$. In this work, we only use lattices with a K point in their Brillouin zone (shown in bold in Table III). In particular, in contrast to Refs. 22–25, we do not use 39-site lattices since they are not compatible with the expected VBC order.

TABLE III. Finite lattices studied in this work. Listed are the number of spins N; the basis vectors **a**, **b** in the xy plane; the diameter $d = \min(|\mathbf{a}|, |\mathbf{b}|, |\mathbf{a} - \mathbf{b}|)$. Lattices shown in bold contain the K point in their Brillouin zone (see Fig. 4 for definition).

Name	**a**	**b**	Diameter
21	$(5/2, \sqrt{3}/2)$	$(1/2, 3\sqrt{3}/2)$	$\sqrt{7}$
24	$(2, \sqrt{3})$	$(-2, \sqrt{3})$	$\sqrt{7}$
27a	$(5/2, \sqrt{3}/2)$	$(-3/2, 3\sqrt{3}/2)$	$\sqrt{7}$
27b	$(3, 0)$	$(3/2, 3\sqrt{3}/2)$	3
30	$(7/2, \sqrt{3}/2)$	$(1/2, 3\sqrt{3}/2)$	$\sqrt{7}$
33	$(5/2, \sqrt{3}/2)$	$(-1, 2\sqrt{3})$	$\sqrt{7}$
36a	$(4, 0)$	$(1/2, 3\sqrt{3}/2)$	$\sqrt{7}$
36b	$(4, 0)$	$(3/2, 3\sqrt{3}/2)$	3
36c	$(-3, \sqrt{3})$	$(3/2, 3\sqrt{3}/2)$	3
36d	$(3, \sqrt{3})$	$(0, 2\sqrt{3})$	$\sqrt{12}$
39a	$(5/2, \sqrt{3}/2)$	$(-3, 2\sqrt{3})$	$\sqrt{7}$
39b	$(5/2, 3\sqrt{3}/2)$	$(-1, 2\sqrt{3})$	$\sqrt{13}$
42a	$(1/2, 3\sqrt{3}/2)$	$(9/2, -\sqrt{3}/2)$	$\sqrt{7}$
42b	$(0, 2\sqrt{3})$	$(7/2, \sqrt{3}/2)$	$\sqrt{12}$
45a	$(5, 0)$	$(3/2, 3\sqrt{3}/2)$	3
45b	$(3, 2\sqrt{3})$	$(-3/2, 3\sqrt{3}/2)$	3
54	$(9/2, 3\sqrt{3}/2)$	$(-3/2, 3\sqrt{3}/2)$	3
63a	$(9/2, \sqrt{3}/2)$	$(3/2, 5\sqrt{3}/2)$	$\sqrt{21}$
63b	$(7, 0)$	$(3/2, 3\sqrt{3}/2)$	3

[1] I. Syôzi, Prog. Theor. Phys. **6**, 306 (1951).

[2] *Introduction to Frustrated Magnetism: Materials, Experiments, Theory*, edited by C. Lacroix, P. Mendels, and F. Mila, Springer Series in Solid-State Sciences (Springer, Berlin, 2011).

[3] C. Zeng and V. Elser, Phys. Rev. B **42**, 8436 (1990); P. Lecheminant, B. Bernu, C. Lhuillier, L. Pierre, and P. Sindzingre, *ibid.* **56**, 2521 (1997); C. Waldtmann, H.-U. Everts, B. Bernu, C. Lhuillier, P. Sindzingre, P. Lecheminant, and L. Pierre, Eur. Phys. J. B **2**, 501 (1998).

[4] G. Evenbly and G. Vidal, Phys. Rev. Lett. **104**, 187203 (2010).

[5] H. Nakano and T. Sakai, J. Phys. Soc. Jpn. **80**, 053704 (2011).

[6] A. M. Läuchli, J. Sudan, and E. S. Sørensen, Phys. Rev. B **83**, 212401 (2011).

[7] O. Götze, D. J. J. Farnell, R. F. Bishop, P. H. Y. Li, and J. Richter, Phys. Rev. B **84**, 224428 (2011).

[8] M. Hermele, Y. Ran, P. A. Lee, and X. G. Wen, Phys. Rev. B **77**, 224413 (2008); Y. Iqbal, F. Becca, and D. Poilblanc, *ibid.* **84**, 020407 (2011); B. Clark, J. Kinder, E. Neuscamman, G. K.-L. Chan, and M. J. Lawler, arXiv:1210.1585.

[9] S. Yan, D. A. Huse, and S. R. White, Science **332**, 1173 (2011).

[10] S. Depenbrock, I. P. McCulloch, and U. Schollwöck, Phys. Rev. Lett. **109**, 067201 (2012).

[11] P. Fazekas and P. W. Anderson, Philos. Mag. **30**, 423 (1974).

[12] H.-C. Jiang, Z. Wang, and L. Balents, Nat. Phys. **8**, 902 (2012).

[13] K. Kanô and S. Naya, Prog. Theor. Phys. **10**, 158 (1953).

[14] R. Moessner, S. L. Sondhi, and P. Chandra, Phys. Rev. Lett. **84**, 4457 (2000); R. Moessner and S. L. Sondhi, Phys. Rev. B **63**, 224401 (2001).

[15] D. C. Cabra, M. D. Grynberg, P. C. W. Holdsworth, A. Honecker, P. Pujol, J. Richter, D. Schmalfuß, and J. Schulenburg, Phys. Rev. B **71**, 144420 (2005).

[16] K. Hida, J. Phys. Soc. Jpn. **70**, 3673 (2001).

[17] J. Schulenburg, A. Honecker, J. Schnack, J. Richter, and H.-J. Schmidt, Phys. Rev. Lett. **88**, 167207 (2002).

[18] J. Richter, J. Schulenburg, and A. Honecker, Lect. Notes Phys. **645**, 85 (2004).

[19] A. Honecker, J. Schulenburg, and J. Richter, J. Phys.: Condens. Matter **16**, S749 (2004).

[20] A. Honecker, D. C. Cabra, M. D. Grynberg, P. C. W. Holdsworth, P. Pujol, J. Richter, D. Schmalfuß, and J. Schulenburg, Phys. B (Amsterdam) **359**, 1391 (2005).

[21] D. C. Cabra, M. D. Grynberg, P. C. W. Holdsworth, and P. Pujol, Phys. Rev. B **65**, 094418 (2002).

[22] H. Nakano and T. Sakai, J. Phys. Soc. Jpn. **79**, 053707 (2010).

[23] T. Sakai and H. Nakano, Phys. Rev. B **83**, 100405(R) (2011).

[24] T. Sakai and H. Nakano, J. Phys.: Conf. Ser. **320**, 012016 (2011).

[25] T. Sakai and H. Nakano, Phys. Status Solidi B **250**, 579 (2013).

[26] Y. Okamoto, M. Tokunaga, H. Yoshida, A. Matsuo, K. Kindo, and Z. Hiroi, Phys. Rev. B **83**, 180407(R) (2011).

[27] H.-J. Schmidt, J. Phys. A **35**, 6545 (2002).

[28] M. E. Zhitomirsky and H. Tsunetsugu, Phys. Rev. B **70**, 100403(R) (2004); Prog. Theor. Phys. Supplement **160**, 361 (2005).

[29] J. Richter, J. Schulenburg, A. Honecker, J. Schnack, and H.-J. Schmidt, J. Phys.: Condens. Matter **16**, S779 (2004); J. Richter, Fiz. Nizk. Temp. (Kharkiv) **31**, 918 (2005) [Low Temp. Phys. **31**, 695 (2005)].

[30] O. Derzhko, J. Richter, A. Honecker, and H.-J. Schmidt, Fiz. Nizk. Temp. (Kharkiv) **33**, 982 (2007) [Low Temp. Phys. **33**, 745 (2007)].

[31] M. B. Hastings, Phys. Rev. B **69**, 104431 (2004).

[32] M. Oshikawa, M. Yamanaka, and I. Affleck, Phys. Rev. Lett. **78**, 1984 (1997).

[33] D. L. Bergman, C. Wu, and L. Balents, Phys. Rev. B **78**, 125104 (2008).

[34] S. D. Huber and E. Altman, Phys. Rev. B **82**, 184502 (2010).

[35] G.-B. Jo, J. Guzman, C. K. Thomas, P. Hosur, A. Vishwanath, and D. M. Stamper-Kurn, Phys. Rev. Lett. **108**, 045305 (2012).

[36] S. A. Parameswaran, I. Kimchi, A. M. Turner, D. M. Stamper-Kurn, and A. Vishwanath, Phys. Rev. Lett. **110**, 125301 (2013).

[37] J. Schnack, H.-J. Schmidt, J. Richter, and J. Schulenburg, Eur. Phys. J. B **24**, 475 (2001).

[38] T. Momoi and K. Totsuka, Phys. Rev. B **61**, 3231 (2000); M. Oshikawa, Phys. Rev. Lett. **84**, 1535 (2000).

[39] J. Richter, O. Derzhko, and J. Schulenburg, Phys. Rev. Lett. **93**, 107206 (2004).

[40] See, for instance, S. Wessel and M. Troyer, Phys. Rev. Lett. **95**, 127205 (2005); D. Heidarian and K. Damle, *ibid.* **95**, 127206 (2005); R. G. Melko, A. Paramekanti, A. A. Burkov, A. Vishwanath, D. N. Sheng, and L. Balents, *ibid.* **95**, 127207 (2005).

[41] S. V. Isakov, S. Wessel, R. G. Melko, K. Sengupta, and Yong Baek Kim, Phys. Rev. Lett. **97**, 147202 (2006).

[42] J. Richter, J. Schulenburg, A. Honecker, and D. Schmalfuß, Phys. Rev. B **70**, 174454 (2004).

[43] G. Misguich and P. Sindzingre, J. Phys.: Condens. Matter **19**, 145202 (2007).

[44] Yan-Zhen Zheng, Ming-Liang Tong, Wei Xue, Wei-Xiong Zhang, Xiao-Ming Chen, Fernande Grandjean, and Gary J. Long, Angew. Chem. Int. Ed. **46**, 6076 (2007).

[45] J. M. Hopkinson and J. J. Beck, arXiv:1207.5836.

[46] I. Rousochatzakis, R. Moessner, and J. van den Brink, arXiv:1305.6488.

[47] R. Siddharthan and A. Georges, Phys. Rev. B **65**, 014417 (2001).

[48] J. Richter, J. Schulenburg, P. Tomczak, and D. Schmalfuß, Condens. Matter Phys. **12**, 507 (2009).

[49] S. Nishimoto, N. Shibata, and C. Hotta, Nat. Commun. **4**, 2287 (2013).